1-3-2022

Stress Corrosion Analysis and Direct Cell Viability of Biodegradable Zn-Fe-Ca Alloy in In-Vitro Conditions

Orit Avior
Ben-Gurion University of the Negev

Noa Ben Ghedalia-Peled
Ben-Gurion University of the Negev

Tomer Ron
Ben-Gurion University of the Negev

Jeremy Goldman
Michigan Technological University, jgoldman@mtu.edu

Razi Vago
Ben-Gurion University of the Negev

See next page for additional authors

Recommended Citation

Avior, O., Ghedalia-Peled, N., Ron, T., Goldman, J., Vago, R., & Aghion, E. (2022). Stress Corrosion Analysis and Direct Cell Viability of Biodegradable Zn-Fe-Ca Alloy in In-Vitro Conditions. *Metals, 12*(1). http://doi.org/10.3390/met12010076
Retrieved from: https://digitalcommons.mtu.edu/michigantech-p/15693

Follow this and additional works at: https://digitalcommons.mtu.edu/michigantech-p

 Part of the Biomedical Engineering and Bioengineering Commons

metals

MDPI

Article

Stress Corrosion Analysis and Direct Cell Viability of Biodegradable Zn-Fe-Ca Alloy in In-Vitro Conditions

Orit Avior [1,*], Noa Ben Ghedalia-Peled [2], Tomer Ron [1], Jeremy Goldman [3], Razi Vago [2] and Eli Aghion [1]

[1] Department of Materials Engineering, Ben-Gurion University of the Negev, Beer-Sheva 8410501, Israel; toron@post.bgu.ac.il (T.R.); egyon@bgu.ac.il (E.A.)
[2] Department of Biotechnology Engineering, Ben-Gurion University of the Negev, Beer-Sheva 8410501, Israel; noabeng@post.bgu.ac.il (N.B.G.-P.); rvago@bgu.ac.il (R.V.)
[3] Biomedical Engineering Department, Michigan Technological University, Houghton, MI 49931, USA; jgoldman@mtu.edu
* Correspondence: oritgree@post.bgu.ac.il

Abstract: Due to the excellent biocompatibility of Zn and Zn-based alloys, researchers have shown great interest in developing biodegradable implants based on zinc. Furthermore, zinc is an essential component of many enzymes and proteins. The human body requires ~15 mg of Zn per day, and there is minimal concern for systemic toxicity from a small zinc-based cardiovascular implant, such as an arterial stent. However, biodegradable Zn-based implants have been shown to provoke local fibrous encapsulation reactions that may isolate the implant from its surrounding environment and interfere with implant function. The development of biodegradable implants made from Zn-Fe-Ca alloy was designed to overcome the problem of fibrous encapsulation. In a previous study made by the authors, the Zn-Fe-Ca system demonstrated a suitable corrosion rate that was higher than that of pure Zn and Zn-Fe alloy. The Zn-Fe-Ca system also showed adequate mechanical properties and a unique microstructure that contained a secondary Ca-reach phase. This has raised the promise that the tested alloy could serve as a biodegradable implant metal. The present study was conducted to further evaluate this promising Zn alloy. Here, we assessed the material's corrosion performance in terms of cyclic potentiodynamic polarization analysis and stress corrosion behavior in terms of slow strain rate testing (SSRT). We also assessed the ability of cells to survive on the alloy surface by direct cell culture test. The results indicate that the alloy develops pitting corrosion, but not stress corrosion under phosphate-buffered saline (PBS) and air environment. The direct cell viability test demonstrates the successful adherence and growth of cells on the alloy surface.

Keywords: biodegradable implants; stress corrosion; direct cell viability; in vitro; zinc; Zn-Fe-Ca

Citation: Avior, O.; Ben Ghedalia-Peled, N.; Ron, T.; Goldman, J.; Vago, R.; Aghion, E. Stress Corrosion Analysis and Direct Cell Viability of Biodegradable Zn-Fe-Ca Alloy in In-Vitro Conditions. *Metals* **2022**, *12*, 76. https://doi.org/10.3390/met12010076

Academic Editor: Dake Xu

Received: 28 November 2021
Accepted: 29 December 2021
Published: 3 January 2022

1. Introduction

The past decade has seen a growing interest in biodegradable implants made of Zn and Zn-alloys [1–6]. The consensus of recent studies has been the potential for Zn and its alloys to serve as a biocompatible structural implant material. Zn exhibits chemical activity with the electrode potential of −0.762 V, falling between the accelerated corrosion of Mg [7,8] with electrode potential of −2.372 V and the insufficient corrosion activity of Fe (−0.444 V) [9]. Zn and its alloys are also attractive for producing implants due to their low melting points, low chemical reactivity, and good machinability [10].

An important consideration for implantable devices that are designed to degrade is that the degradation byproducts have beneficial uses within the host system. Indeed, ionic Zn is a component of hundreds of enzymes and proteins. Furthermore, optimal nucleic acids, protein metabolism, cell growth, division and function require sufficient availability of ionic Zn [11]. The human body contains 2–3 g of Zn, and nearly 90% is found in muscle and bone [11]. The daily allowance of Zn in the human body is 15 mg/day [12], and the body is able to absorb this amount from the environment, regulate its concentration

in body fluids, transport it safely throughout the body, and excrete excess amounts [11]. Therefore, there is minimal concern for systemic side effects [9] from the ionic Zn byproduct of Zn-based implants, particularly from small devices such as arterial stents.

The mechanical properties of pure Zn suffer from low strength (σ_{UTS} below 20 MPa) and reduced ductility (ε of 0.2%) that are insufficient for most medical applications [13]. Not surprisingly, many studies have been performed to improve the strength of pure Zn through conventional metallurgical approaches, including alloying. Among these alloys include Zn-Mg [14], Zn-Ca and Zn-Sr [15], Zn-Fe-Mg [16], Zn-Mg-Sr [17], Zn-Mg-Mn [18], Zn-Fe [19]. These alloys exhibit increased strength, although the degradation rates are still too low or, in some cases, too high to serve as biodegradable implants. Importantly, Zn-based implants with insufficient degradation rates may elicit fibrous encapsulation responses that interfere with the implant's function [20].

Another very important aspect that needs to be addressed as part of the development process of biodegradable Zn-based implants is their resistance to stress corrosion failure in in-vivo conditions. Stress corrosion cracking (SCC) is one of the major reasons for premature implant failure, for example, in orthopedic applications [21]. This is mainly due to the combined effect of external loading and corrosive physiological environment [22].

The present study continued to investigate the feasibility of using Zn-Fe-Ca alloy to produce biodegradable implants. Fe is an essential nutrient element in the human body and plays an important role in vital biochemical activities, such as oxygen sensing and transport, electron transfer and catalysis [23]. Therefore, the release of ionic Fe from the degrading implant may be beneficial for the host system. Ca is an essential bone constituent and one of the vital elements in the human body [24]. Therefore, there is little concern for systemic toxicity from Ca release from the degrading material. Furthermore, the amount of Ca alloyed into the tested alloy (0.6%) is systemically negligible relative to the 0.8 g daily allowance in the human body [12].

The overall goal of these studies is to develop Zn-based implant metals with suitable mechanical properties and corrosion behavior for clinical applications that avoid fibrous encapsulation (degradation rate too low) or local toxicity (degradation rate too high) responses. In an earlier contribution, the mechanical properties, environmental behavior, and indirect cell viability of Zn-Fe-Ca alloys containing different concentrations of Ca were examined [25]. In the present study, the effect of strain rate on stress corrosion resistance of Zn-Fe-Ca alloy and the direct cell viability was tested. This study aims to ensure that the Zn-Fe-Ca alloy does not develop stress corrosion in a physiological environment and that there is a possibility of tissues growth around the implant. This is to enable the research to progress to in vivo tests.

2. Materials and Methods

The experimental program included the casting of alloys, microstructure analysis, followed by the preparation of suitable models for each experiment. Several tests were designed to test the resistance of the alloy to stress corrosion and to grow cells directly on the alloy. For each test, at least three models were prepared, and three repetitions were performed for statistical analysis.

2.1. Alloy Preparation

An alloy with the composition of Zn-2%Fe-0.6%Ca was prepared by gravity casting. The Ca concentration was selected due to its embrittlement effect on Zn-based alloys. A previous article by the author [25] examined the mechanical properties of Zn-based alloys with Ca inclusions. The results showed that extrusion could not be performed on alloys containing more than 0.6% Ca. Therefore, a calcium concentration of 0.6% was selected for the present alloy. The cast was performed in a graphite crucible using pure Zn ingots (99.99%), pure Fe (99%) with powder size up to 44 microns (−325 mesh) and pure Ca in the form of granules. The alloying process was performed at 750 °C for 3 h along with active stirring every 30 min. The molten alloy was cast as bars in rectangular steel die with the

following dimensions: 6 cm × 6 cm × 15 cm. The as-cast bars were machined to obtain rods with 13 mm diameter and then extruded with a 1:5 ratio. Prior to the extrusion process, the rods were preheated to 350 °C. A final dimension of 6 mm diameter was obtained for the rods.

2.2. Microstructure Characterization

X-ray diffraction analysis was performed by an X-ray diffractometer (RIGAKU-2100H (RIGAKU, Tokyo, Japan) with Cu-Kα. Diffraction patterns were generated between 10–90° at 40 kV, 30 mA, and a scanning rate of 0.02°/min. The relatively reduced scanning rate aims at detecting small modifications in the microstructure created by the minor addition of calcium to the tested alloy. Microstructural analysis was carried out using a JEOL JSM-5600 (JEOL, Tokyo, Japan) scanning electron microscope (SEM) equipped with an Energy-dispersive X-ray spectroscopy (EDS) detector (Thermo Fisher Scientific, Waltham, MA, USA) for spot chemical analysis [26]. All the tested samples for SEM evaluation were polished and etched using a 5% Nital (5 mL HNO_3 + 100 mL ethanol) solution.

2.3. Cyclic Potentiodynamic Polarization

The Electrochemical behavior was evaluated in terms of cyclic potentiodynamic polarization and carried out using a Bio-Logic SP-200 potentiostat equipped with EC-Lab software V11.18. The three-electrode cell method used for the test included a saturated calomel reference electrode (SCE), a platinum counter electrode, and the tested sample as a working electrode. The exposed area of the working electrode was 1 $cm^{2,}$ and the test solution was phosphate-buffered saline (PBS) at ambient temperature. The PBS solution was produced from one standard tablet of PBS and 200 mL of deionized water, which consequently contained the concentration of 0.01 M phosphate buffer, 0.0027 M potassium chloride, and 0.137 M sodium chloride. Based on the previous experience of the authors [25], the potential scanning rate was selected as 1 mV/s, and the corrosion rates were calculated by Tafel extrapolation. The test was performed three times for statistical analysis.

2.4. Slow Strain Rate Tensile (SSRT)

The stress corrosion behavior in terms of SSRT was performed at room temperature using a CORMET slow strain rate machine (C76, Cormet Testing Systems, Vantaa, Finland). The SSRT analysis was carried in PBS solution at 37 °C and in the air (for reference considerations) at strain rates of 2.5×10^{-5}, 2.5×10^{-6}, 2.5×10^{-7} S^{-1}. The tested samples with a rod shape had a diameter of 8 mm, and a total length of 70 mm. The gauge length was 16 mm length with a diameter of 4 mm. The tested samples were inserted in a cylindrical chamber containing PBS corrosive solution that was attached to the SSRT testing system. The test was performed three times for each strain rate.

2.5. Direct Incubation of Cells on Zn-2%Fe-0.6%Ca Alloy

Direct cell testing was performed to evaluate cell adhesion and viability on the alloy surface. Sample preparation and the experimental protocol were carried out according to ISO 10993-5/12 standards [27,28]. Mus musculus (mouse) 4T1 cells were culture in an incubator under a humidified atmosphere with 5% CO_2 at 37 °C using Dulbecco Modified Eagle's Medium (DMEM) supplemented with 4.5 g L^{-1} D-Glucose, 10% Fetal Bovine Serum (FBS), 4 mM L-Glutamine, 1 mM Sodium Pyruvate, and 1% Penicillin Streptomycin Neomycin (PSN) antibiotic mixture (Biological Industry, Beit Haemek, Israel). In total, 4T1 cells were selected due to their homogeneity and rapid proliferation with maintained properties following each passage. This reduces experimental variability relative to primary cells. It also facilitates a direct comparison of results between experiments and different studies [29]. Cylindrical samples (D = 10 mm, h = 2 mm) made from a Zn-2%Fe-0.6%Ca alloy and a Ti-6Al-4V reference alloy (control group) were prepared using four samples from each alloy for each of the two independent repetitions of the experiment. Prior to the experiment, the samples were polished up to 2500 grit, ultrasonically cleaned for 5 min in

ethanol and 2 min in acetone, and then air-dried followed by sterilization in an autoclave. All the samples were pre-incubated for 24 h in Dulbecco Modified Eagle's Medium (DMEM) at 37 °C in a humidified atmosphere. The surface area to volume ratio of the culture medium was 1.25 cm^2 mL^{-1}, according to the standards. After the pre-incubation, the samples were placed in 24-well cell culture plates. Subsequently, the cells were seeded directly onto the sample surface at a density of 50,000 cells per well. DMEM was added to each well according to the required standard ratio. The plates were incubated under a humidified atmosphere with 5% CO_2 at 37 °C for 24 and 48 h.

The number of adherent cells was visualized using NucBlue™ Live Cell Stain Formulation kit (RHENIUM, Modi'in, Israel) and then documented by a CoolLED pe-2 collimator fitted to an inverted phase-contrast microscope (Eclipse Ti, Nikon) equipped with a digital camera (D5-Qi1Mc, Nikon, Tokyo, Japan) using the appropriate fluorescent filters. Cell adhesion per unit field was quantified by averaging cell counts at three random locations on the sample surface.

Cell viability was evaluated using a Live and Dead Cell Assay (Abcam, Cambridge, UK) following the manufacturer's protocol. The Live and Dead Assay stain solution is a mixture of two highly fluorescent dyes that differentially label live and dead cells: The live cell dye labels intact, viable cells green. It is membrane-permeant and non-fluorescent until ubiquitous intracellular esterases remove ester groups and render the molecule fluorescent. The Excitation (max) and Emission (max) are 494 nm and 515 nm, respectively. The dead cell dye labels cells with compromised plasma membranes red. It is membrane-impermeant and binds to DNA with high affinity. Once bound to DNA, the fluorescence increases >30-fold. The excitation (max) and emission (max) are 528 nm and 617 nm, respectively [30].

3. Results

Three phases were found in the results of the X-ray diffraction analysis: pure Zn, a Fe-rich phase, and a Ca-rich phase, as shown in Figure 1. The Fe-rich phase was identified as $Zn_{11}Fe$ (according to ICDD 045-1184), and the Ca-rich phase was identified as $CaZn_{13}$ (according to ICDD 028-0258).

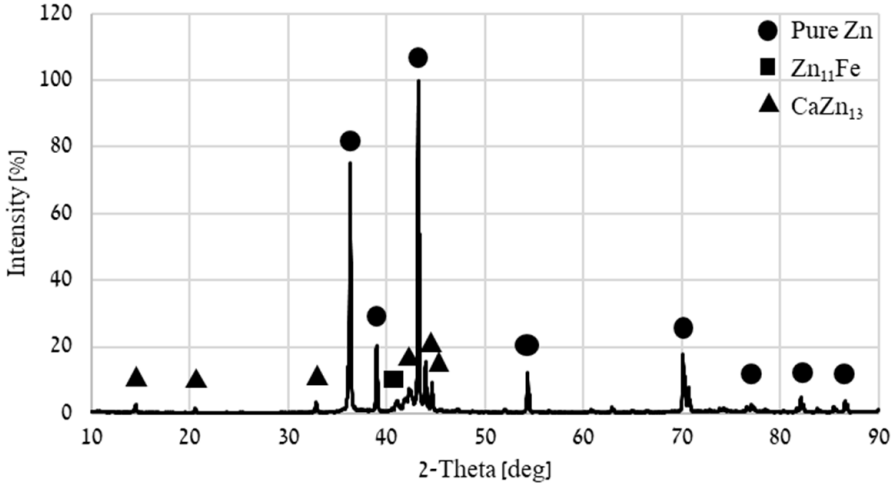

Figure 1. XRD diffraction analysis of Zn-2%Fe-0.6%Ca alloy.

Figure 2 and Table 1 show the typical microstructure obtained by SEM and EDS analysis results. The microstructure of the ternary alloy contains the Fe-rich phase ($Zn_{11}Fe$) and Ca-rich phase ($CaZn_{13}$) in addition to the pure Zn matrix, as also shown in the previous article of the author [25]. In this composition, the Ca-rich phase is present in the form of a three-petaled flower.

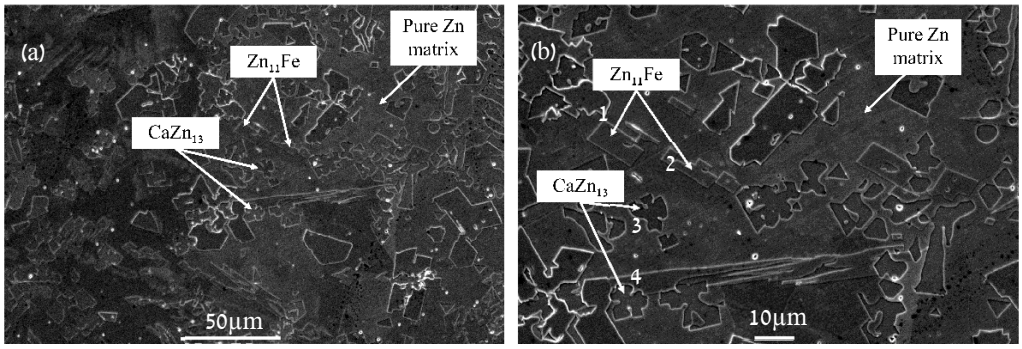

Figure 2. Typical microstructure of biodegradable Zn-2%Fe-0.6%Ca alloy obtained by SEM in two different magnifications (**a**) X500, (**b**) X1000.

Table 1. EDS results summary.

Point	Ca [wt.%]	Fe [wt.%]	Zn [wt.%]
1	0.00 ± 0.00	6.36 ± 0.38	93.64 ± 1.79
2	0.00 ± 0.07	5.60 ± 0.37	94.39 ± 1.74
3	4.20 ± 0.14	0.36 ± 0.15	95.45 ± 1.78
4	4.25 ± 0.14	0.11 ± 0.15	95.65 ± 1.78

The general corrosion behavior of the tested alloy under in vitro conditions is shown in the previous paper of the author, which included the following results: E_{OC} of −1.06 V, corrosion parameters from potentiodynamic polarization analysis: E_{CORR} [V] of −1.1287, I_{CORR} [µA/cm^2] of 0.41, and Corrosion rate [mmpy] of 0.0062 [25]. In order to try and evaluate the sensitivity of the tested alloy to localized corrosion attack, cyclic potentiodynamic polarization was performed, although this research tool is mainly applicable to metals with clear passivation characteristics. The results are shown in Figure 3, and the Tafel extrapolation measurements are shown in Table 2. As expected, the corrosion parameters are similar to those obtained in the potentiodynamic polarization of the previous study. The cyclic potentiodynamic polarization results show a hysteresis curve that may indicate that the alloy is sensitive to pitting corrosion attack [31].

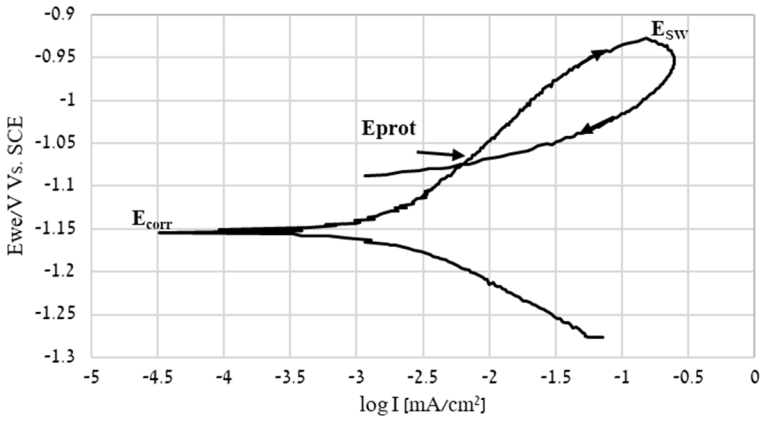

Figure 3. Typical cyclic potentiodynamic polarization analysis of Zn-2%Fe-0.6%Ca alloy in PBS solution.

Table 2. Tafel extrapolation measurements obtained from the cyclic potentiodynamic poilarization analysis.

Corrosion Parameter	E_{CORR} [V]	I_{CORR} [µA/cm^2]	Corrosion Rate [mmpy]
	−1.1575 ± 0.0064	0.332 ± 0.065	0.0049 ± 0.0010

Stress corrosion examination of the tested alloy and reference metal by slow strain rate testing (SSRT) in PBS and air is shown in Figure 4. The PBS and air curves were relatively similar for all the strain rates apart from slight elongation loss in the PBS solution. The minor stress drops that accrue along the stress–strain curves can be related to inherent defects generated during the solidification phase of the tested alloy.

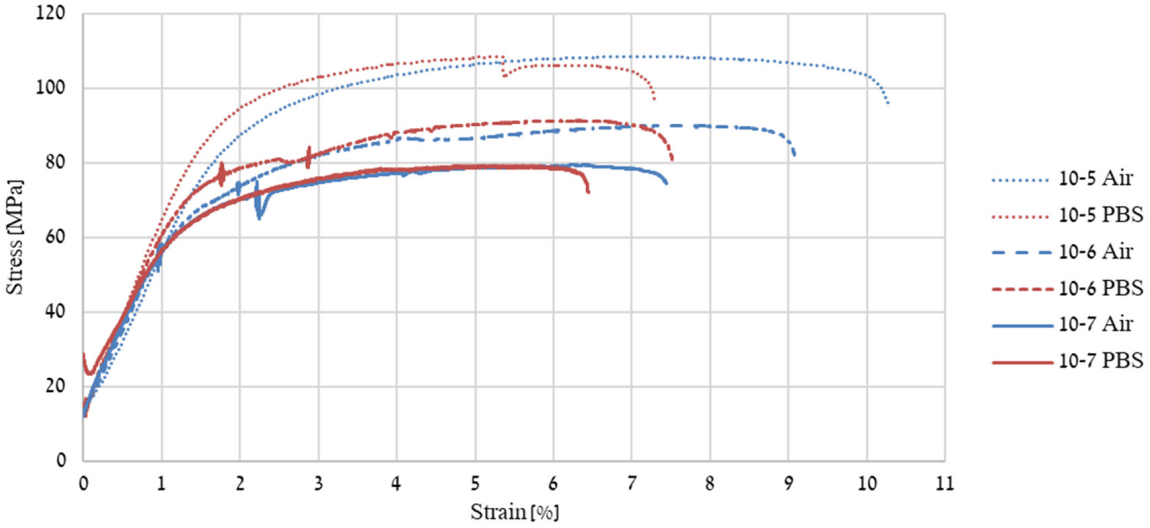

Figure 4. Typical stress–strain curves of Zn-2%Fe-0.6%Ca alloy in air and PBS solution for strain rates between 10^{-5} to 10^{-7} S^{-1}.

Stress corrosion analyses in terms of ultimate tensile strength (UTS) and yield point (YP) vs. strain rate are shown in Figures 5 and 6, respectively. As expected from the SSRT stress–strain curves, the UTS and YP increased with the increase of the strain rate, although the values in PBS and air are almost identical, with similar trend lines in the UTS figure. The fitting equation of this trend line is $\sigma_{UTS} = c \times \varepsilon^m$ [32], while the strain rate sensitively factor (m) of the alloy in PBS and air were very close: 0.06, 0.07, respectively. It can therefore be determined that the strength of the alloy do not suffer from stress corrosion. However, the slight elongation loss in PBS solution, as shown in Figure 7, may signify some stress corrosion sensitivity which did not have a significant effect on time to failure vs. strain rate in both environmental conditions, as shown in Figure 8.

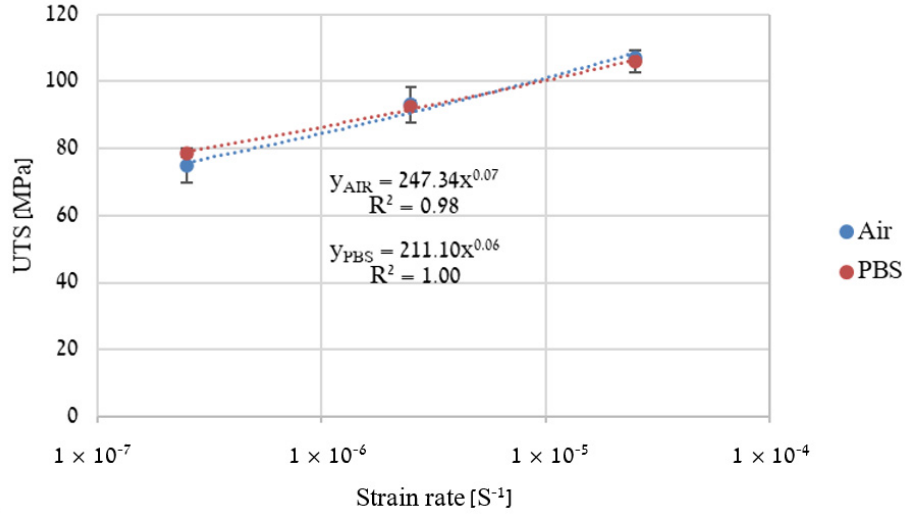

Figure 5. UTS vs. strain rate of Zn-2%Fe-0.6%Ca alloy in air and PBS solution.

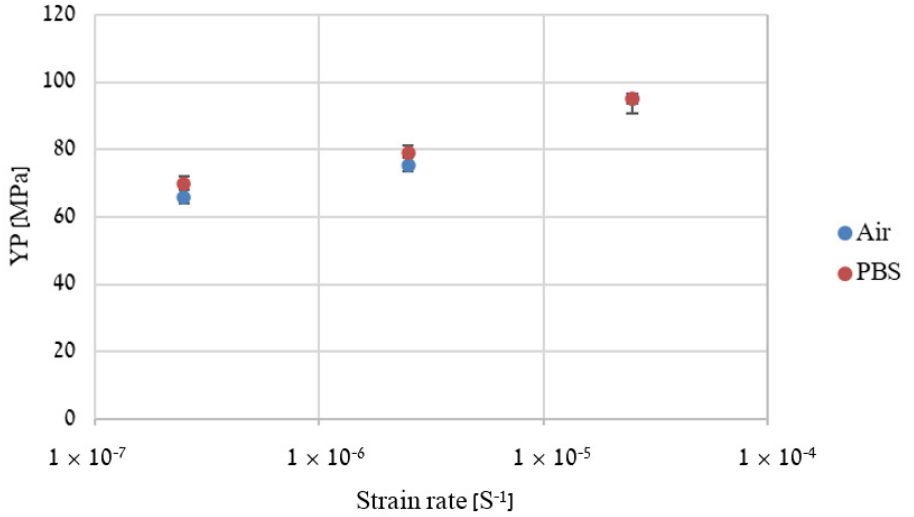

Figure 6. Yield point vs. strain rate of Zn-2%Fe-0.6%Ca alloy in air and PBS solution.

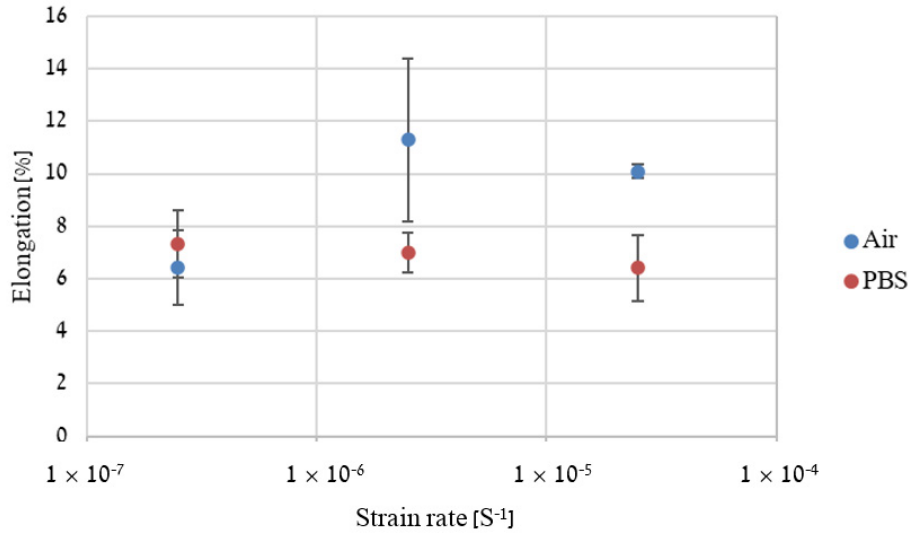

Figure 7. Elongation vs. strain rate of Zn-2%Fe-0.6%Ca alloy in air and PBS solution.

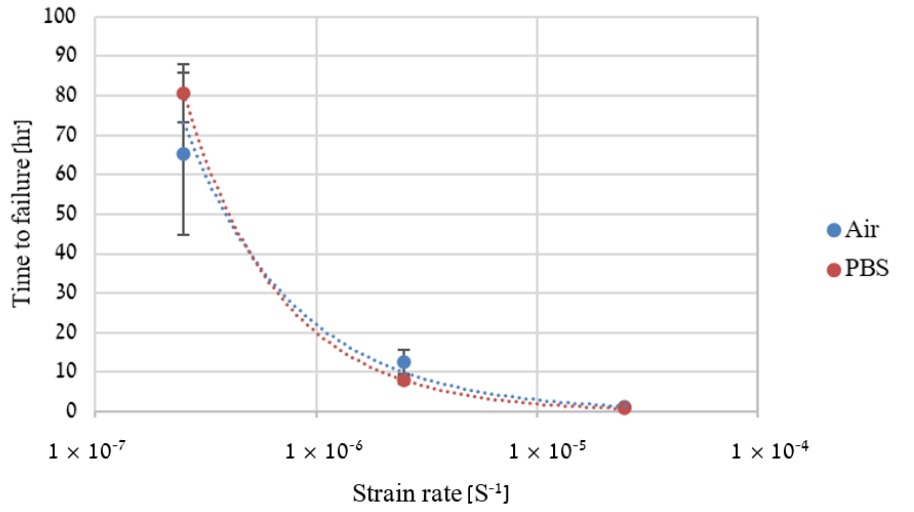

Figure 8. Time to failure vs. strain rate of Zn-2%Fe-0.6%Ca alloy in air and PBS solution.

Fractography analysis obtained by SEM is shown in Figure 9. All fractures are intergranular fractures, which is an expected embrittlement effect due to the presence of Ca. Altogether the fact that the performance of Zn-2%Fe-0.6%Ca alloy under SSRT conditions in air and PBS solution was quite similar clearly indicate that the sensitivity of this alloy to stress corrosion in a simulated physiological environment is insignificant.

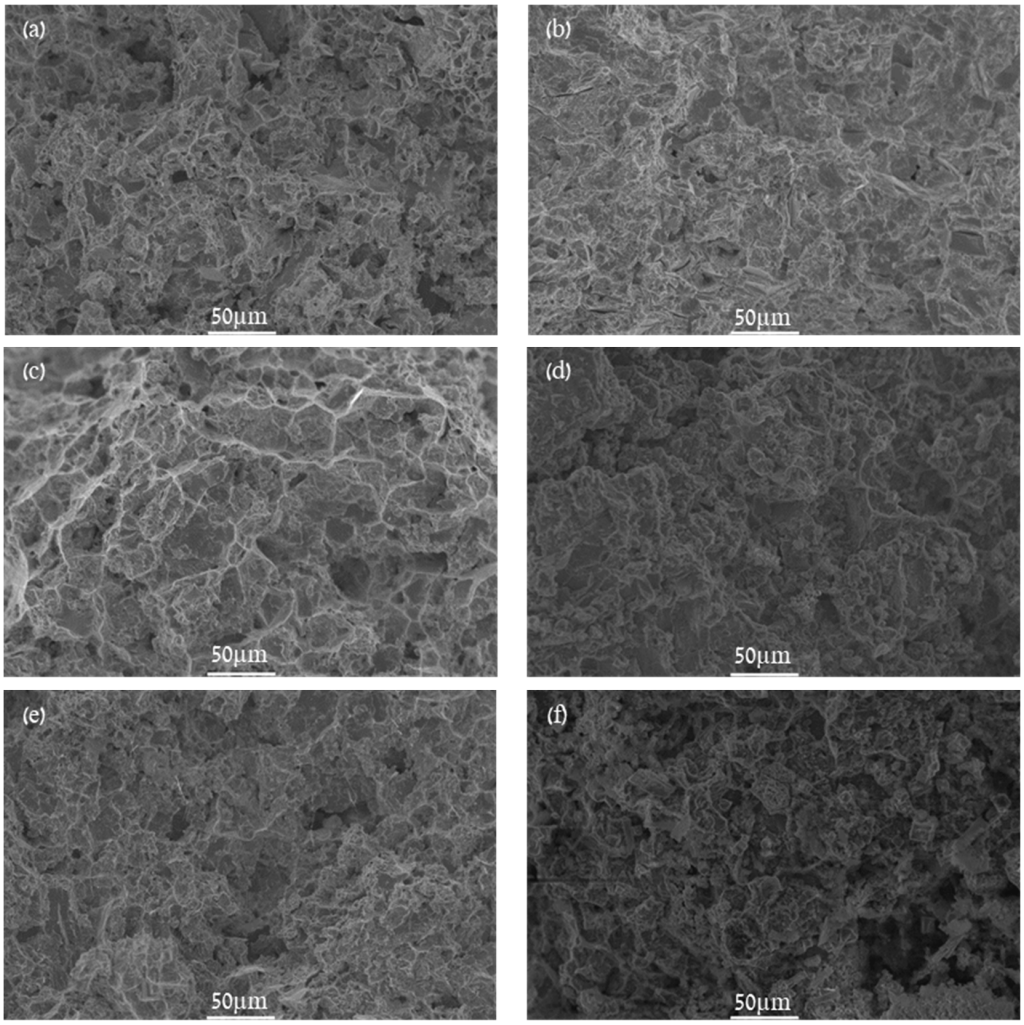

Figure 9. Typical fracture surface images after tensile testing of Zn-2%Fe-0.6%Ca alloy in PBS solution and air, respectively, at various strain rates. (**a**,**b**) $2.5 \cdot 10^{-5}$ S^{-1}; (**c**,**d**) $2.5 \cdot 10^{-6}$ S^{-1}; (**e**,**f**) $2.5 \cdot 10^{-7}$ S^{-1}.

The ability of cells to adhere and remain viable on the surface of the alloy is critical information for determining the ability of the alloy to serve as a biodegradable implant. The adherent cells on the surface of Zn-2%Fe-0.6%Ca and Ti_6Al_4V alloys are shown in Figure 10. It is apparent that the number of cells increases from 24 to 48 h in both the tested alloy and reference metal. This demonstrates that the cells were able to adhere and proliferate on the surface of the alloy.

The number of adherent cells per unit field on the alloy surfaces was counted, as presented in Figure 11. Although more cells were able to adhere to the biostable reference metal, the number of adherent cells increased two-fold from 24 to 48 h for both materials. The ability of cells to adhere and proliferate on the Zn-alloy surface demonstrates its suitable biocompatibility.

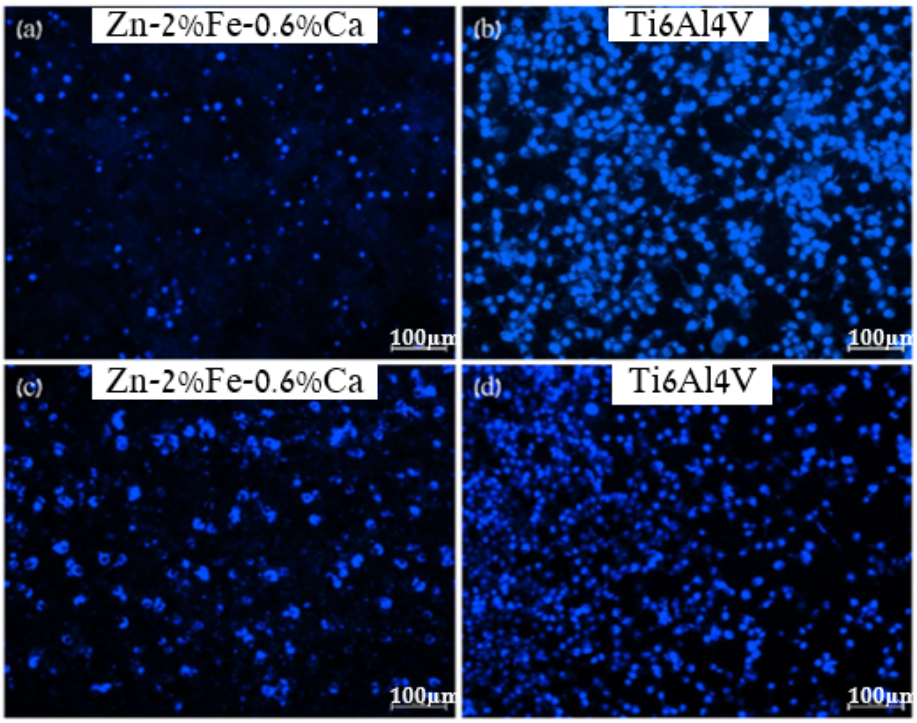

Figure 10. Typical fluorescence micrographs of NucBlue stained 4T1 cells attached to the surface of Zn-2%Fe-0.6%Ca and Ti6Al4V alloy, respectively (**a**,**b**) after 24 h of incubation; (**c**,**d**) after 48 h of incubation.

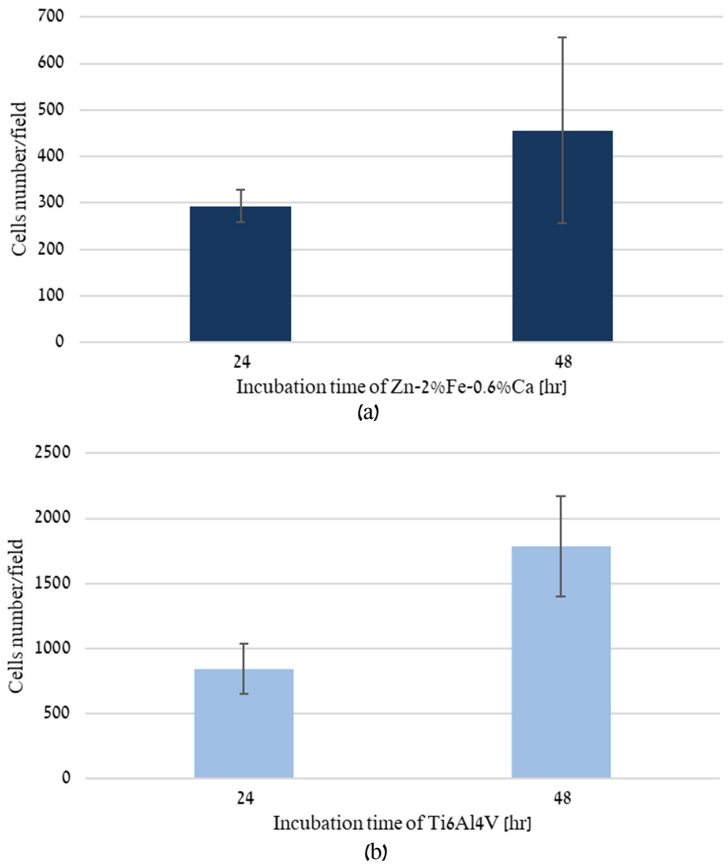

Figure 11. Typical number of cells per unit field after 24 and 48 h of incubation (**a**) Zn-2%Fe-0.6%Ca, (**b**) Ti6Al4V.

Cell viability and adhesion were further investigated using the Live and Dead Cell Assay for both Zn-2%Fe-0.6%Ca and Ti6Al4V alloys, as shown in Figure 12. The 4T1 cells demonstrate the normal appearance of live cells (green) with only a few dead cells (red) on both alloys after 24 h. Hardly any dead cells are seen on the surface after 48 h, likely because dead cells lose their surface adhesion and are washed in the DMEM.

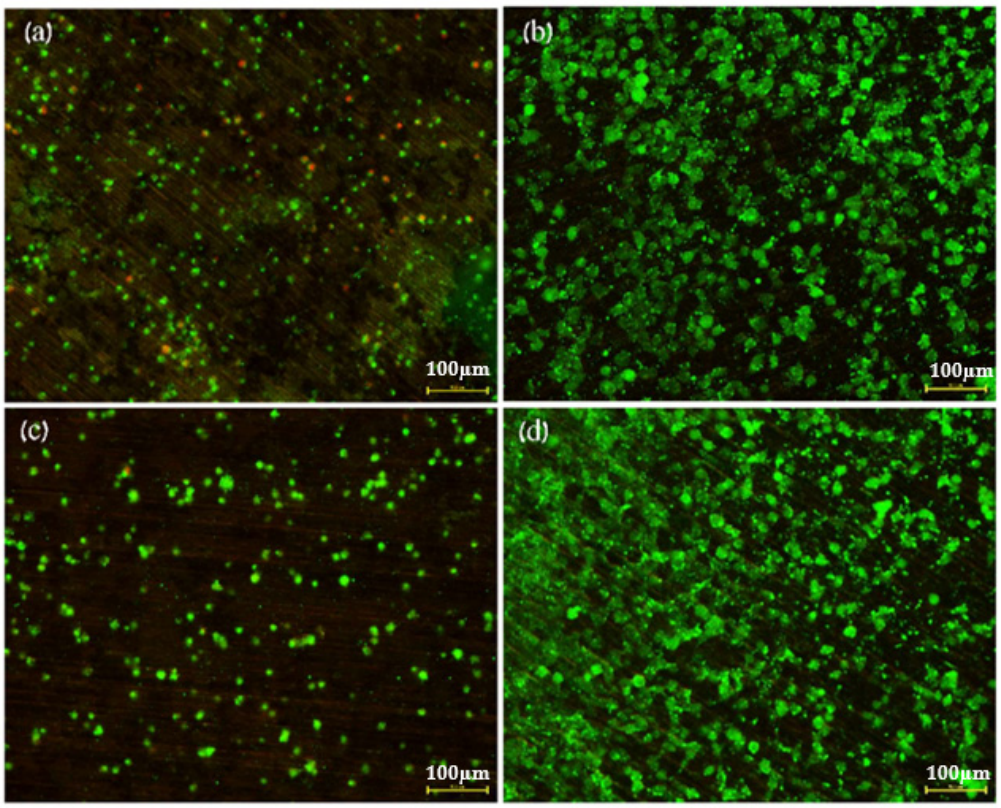

Figure 12. Typical fluorescence images of live (green) and dead (red) 4T1 cells attached to Zn-2%Fe-0.6%Ca and to Ti6Al4V, respectively (**a**,**b**) after 24 h incubation; (**c**,**d**) after 48 h incubation.

The reduction in cell adhesion and growth on Zn-2%Fe-0.6%Ca alloy compared to the reference metal may be attributed to the release and accumulation of Zn^{2+} cations near the surface of the alloy during the incubation period. It is a well-known property of Zn implants that cells are viable at the surface under in vivo conditions but experience some degree of local toxicity under in vitro conditions [33]. In this context, the increased cell numbers on the alloy surface from 24 to 48 h demonstrates the good biocompatibility of the new alloy.

4. Discussion

Zn-based implants that are being developed may exhibit disadvantageous properties in terms of biodegradation characteristics in physiological environments. Specifically, low degradation rates for Zn and Zn-based alloys may provoke inflammation and fibrous encapsulation responses [20], which hinder implant function and integration into the surrounding biological environment. High degradation rates may provoke cytotoxicity. The first part of our study showed that the addition of Ca to Zn-Fe alloy increased the degradation rate (from ~0.3 mmpy in pure Zn to ~0.57 mmpy in alloy contained 0.6% Ca [25]), achieved good mechanical properties, and was not cytotoxic by evaluation in an indirect cell culture test [25]. The potential of the $CaZn_{13}$ phase is lower than that of pure Zn. Hence, the $CaZn_{13}$ phase acts as the cathode in the Zn alloys, accelerating the corrosion of the alloy through the micro galvanic effect [34]. An increase in the degradation rate is vital for avoiding fibrous encapsulation of Zn-based implants [20].

The present study demonstrates that Zn-2%Fe-0.6%Ca alloy nearly avoids stress corrosion deficiencies and permits cell growth directly on the surface. The very similar UTS, YP, and time to failure values in PBS and air under different strain rates suggest that prior to natural degradation, the tested alloy will not experience a premature failure due to stress corrosion effects. This is mainly related to the critical service period where the implant should maintain its mechanical integrity. In parallel, it is believed that the relatively slight elongation loss in PBS solution can have only a minor effect on the overall stress corrosion performance. The microstructure analysis revealed that in the tested alloy, there are two phases that create a micro-galvanic effect between them and the Zn matrix. Previous research revealed that micro-galvanic corrosion along grain boundaries is a major factor affecting stress corrosion crack (SCC) [35]. In this context, we would expect that the development of stress corrosion will take place at the grain boundaries of the tested alloy. The fractography analysis in Figure 9 shows that the nature of the fractures was inter-granular without any significant oxidation. This comes in line with other studies [35,36], which indicate that plastic deformation such as extrusion, as performed by this study, may reduce the micro-galvanic effect of the secondary phases on SCC performance due to their homogenized distribution.

A critical feature of a biodegradable implant is that the implant should be biocompatible. Therefore, the alloying elements should be functionally inert [37] or preferably have a beneficial effect on the body. In this study, the tested Zn-based alloy contains Fe and Ca as alloying elements. These two elements are not just biocompatible materials, but they also provide beneficial effects on the human body functions as they are released from the degrading implant [13]. For instance, Zn is considered to be an anti-bacterial and anti-viral element [38,39], Ca is an important element for skeleton development and for maintaining bone mass [13,37,40], and Fe has a crucial role in the respiratory process. In this study, the ability of cells to grow on the tested alloy surface was examined in terms of direct cell viability analysis. The obtained results suggest that the increased corrosion rate of the alloy will not produce any toxic accumulation of Zn ions at the implant surface. It should be noted that the direct cell viability test showed reduced numbers of cells on the surface of the Zn alloy relative to the reference Ti-base alloy. This phenomenon may be due to the inevitable accumulation of Zn^{2+} cations on the alloy surface during degradation under in vitro conditions. Such a mild effect is not expected to be a limitation under in vivo conditions due to endogenous buffering and clearance mechanisms. Moreover, there is a good possibility that these Zn cations can promote healing processes of the biological matrix in the vicinity of the biodegradable implant by preventing undesired inflammations. Altogether, the results suggest that biodegradable implants made from the tested alloy may be able to serve as a mechanical scaffold for biomedical applications. Research efforts should proceed to in vivo testing of the alloy.

5. Conclusions

The tested alloy Zn-2%Fe-0.6%Ca was not sensitive to stress corrosion under the simulated physiological environment. The tested alloy is suitable for cell growth under in vitro conditions, as seeded cells were adherent and viable on the alloy surface. Consistent with other in vitro studies, we have found that the rate of cell adhesion and growth is reduced on the surface of Zn-based alloys.

Author Contributions: Designed the experiments and wrote the paper: E.A. and O.A.; performed the experiments: O.A.; assisted with the experiments: T.R.; assisted with the experiments relating to direct incubation of cells: N.B.G.-P. and R.V. Investigation: J.G. All authors have read and agreed to the published version of the manuscript.

Funding: This research received no external funding.

Institutional Review Board Statement: Not applicable.

Informed Consent Statement: Not applicable.

Conflicts of Interest: The authors declare no conflict of interest.

References

1. Seitz, J.M.; Durisin, M.; Goldman, J.; Drelich, J.W. Recent advances in biodegradable metals for medical sutures: A critical review. *Adv. Healthc. Mater.* **2015**, *4*, 1915–1936. [CrossRef]
2. Wang, C.; Yang, H.; Li, X.; Zheng, Y. In vitro evaluation of the feasibility of commercial Zn alloys as biodegradable metals. *J. Mater. Sci. Technol.* **2016**, *32*, 909–918. [CrossRef]
3. Törne, K.; Larsson, M.; Norlin, A.; Weissenrieder, J. Degradation of zinc in saline solutions, plasma, and whole blood. *J. Biomed. Mater. Res. Part B* **2016**, *104*, 1141–1151. [CrossRef] [PubMed]
4. Bolz, A.; Popp, T. Implantable, Bioresorbable VesselWall Support, in Particular Coronary Stent. U.S. Patent 6,287,332 B1, 11 September 2001.
5. Zhou, G.; Gongqi, Q.; Gong, H. Kind of Absorbable High Strength and Toughness Corrosion-Resistant Zinc Alloy Implant Material for Human Body. U.S. Patent 20,170,028,107 A1, 2 February 2017.
6. Yang, H.; Jia, B.; Zhang, Z.; Qu, X.; Li, G.; Lin, W.; Zheng, Y. Alloying design of biodegradable zinc as promising bone implants for load-bearing applications. *Nat. Commun.* **2020**, *11*, 1–16.
7. Aghion, E.; Bronfin, B.; Eliezer, D.; Von Buch, F.; Schumann, S.; Friedrich, H. The Art of Developing New Magnesium Alloys for High Temperature Applications. *Mater. Sci. Forum* **2003**, *419–422*, 407–418. [CrossRef]
8. Aghion, E.; Gueta, Y.; Moscovitch, N.; Bronfin, B. Effect of yttrium additions on the properties of grain-refined Mg–3% Nd alloy. *J. Mater. Sci.* **2008**, *43*, 4870–4875. [CrossRef]
9. Liu, X.; Sun, J.; Qiu, K.; Yang, Y.; Pu, Z.; Li, L.; Zheng, Y. Effects of alloying elements (Ca and Sr) on microstructure, mechanical property and in vitro corrosion behavior of biodegradable Zn–1.5Mg alloy. *J. Alloy. Compd.* **2016**, *664*, 444–452. [CrossRef]
10. Niu, J.; Tang, Z.; Huang, H.; Pei, J.; Zhang, H.; Yuan, G.; Ding, W. Research on a Zn-Cu alloy as a biodegradable material for potential vascular stents application. *Mater. Sci. Eng. C* **2016**, *69*, 407–413. [CrossRef]
11. Plum, L.M.; Rink, L.; Haase, H. The essential toxin: Impact of zinc on human health. *Int. J. Environ. Res. Public Health* **2010**, *7*, 1342–1365. [CrossRef]
12. Zheng, Y.; Gu, X.; Witte, F. Biodegradable metals. *Mater. Sci. Eng. C* **2014**, *77*, 1–34. [CrossRef]
13. Li, H.; Yang, H.; Zheng, Y.; Zhou, F.; Qiu, K.; Wang, X. Design and characterizations of novel biodegradable ternary Zn-based alloys with iia nutrient alloying elements mg, ca and sr. *Mater. Des.* **2015**, *83*, 95–102. [CrossRef]
14. Dambatta, M.S.; Izman, S.; Kurniawan, D.; Farahany, S.; Yahaya, B.; Hermawan, H. Influence of thermal treatment on microstructure, mechanical and degradation properties of Zn–3Mg alloy as potential biodegradable implant material. *Mater. Des.* **2015**, *85*, 431–437. [CrossRef]
15. Li, H.F.; Xie, X.H.; Zheng, Y.F.; Cong, Y.; Zhou, F.Y.; Qiu, K.J.; Qin, L. Development of biodegradable Zn-1X binary alloys with nutrient alloying elements Mg, Ca and Sr. *Sci. Rep.* **2015**, *5*, 1–14.
16. Wang, C.; Yu, Z.; Cui, Y.; Zhang, Y.; Yu, S.; Qu, G.; Gong, H. Processing of a novel Zn alloy micro-tube for biodegradable vascular stent application. *J. Mater. Sci. Technol.* **2016**, *32*, 925–929. [CrossRef]
17. Liu, X.; Sun, J.; Yang, Y.; Zhou, F.; Pu, Z.; Li, L.; Zheng, Y. Microstructure, mechanical properties, in vitro degradation behavior and hemocompatibility of novel Zn–Mg–Sr alloys as biodegradable metals. *Mater. Lett.* **2016**, *162*, 242–245. [CrossRef]
18. Liu, X.; Sun, J.; Zhou, F.; Yang, Y.; Chang, R.; Qiu, K.; Zheng, Y. Micro-alloying with Mn in Zn–Mg alloy for future biodegradable metals application. *Mater. Des.* **2016**, *94*, 95–104. [CrossRef]
19. Kafri, A.; Ovadia, S.; Yosafovich-Doitch, G.; Aghion, E. The Effects of 4%Fe on the Performance of Pure Zinc as Biodegradable Implant Material. *Ann. Biomed. Eng.* **2019**, *47*, 1400–1408. [CrossRef]
20. Guillory, R.J.; Bowen, P.K.; Hopkins, S.P.; Shearier, E.R.; Earley, E.J.; Gillette, A.A.; Aghion, E.; Bocks, M.L.; Drelich, J.W.; Goldman, J. Corrosion characteristics dictate the long-term inflammatory profile of degradable zinc arterial implants. *ACS Biomater. Sci. Eng.* **2016**, *2*, 2355–2364. [CrossRef]
21. Aksakal, B.; Yildirim, Ö.S.; Gul, H. Metallurgical failure analysis of various implant materials used in orthopedic applications. *J. Fail. Anal. Prev.* **2004**, *4*, 17–23. [CrossRef]
22. Li, H.F.; Shi, Z.Z.; Wang, L.N. Opportunities and challenges of biodegradable Zn-based alloys. *J. Mater. Sci. Technol.* **2020**, *46*, 136–138. [CrossRef]
23. Huang, T.; Cheng, J.; Zheng, Y.F. In vitro degradation and biocompatibility of Fe–Pd and Fe–Pt composites fabricated by spark plasma sintering. *Mater. Sci. Eng. C* **2014**, *35*, 43–53. [CrossRef]
24. Kwok, S.C.H.; Ha, P.C.T.; McKenzie, D.R.; Bilek, M.M.M.; Chu, P.K. Biocompatibility of calcium and phosphorus doped diamond-like carbon thin films synthesized by pla sma immersion ion implantation and deposition. *Diam. Relat. Mater.* **2006**, *15*, 893–897. [CrossRef]
25. Avior, O.; Ben Ghedalia-Peled, N.; Ron, T.; Vago, R.; Aghion, E. The Effect of Ca on In Vitro Behavior of Biodegradable Zn-Fe Alloy in Simulated Physiological Environments. *Metals* **2020**, *10*, 1624. [CrossRef]
26. Kaya, A.; Uzan, P.; Eliezer, D.; Aghion, E. Electron microscopical investigation of as cast AZ91D alloy. *Mater. Sci. Technol.* **2000**, *16*, 1001–1006. [CrossRef]
27. ISO-10993-5. *Biological Evaluation of Medical Devices, Part 5: Tests for in Vitro Cytotoxicity. International Organization for Standardization*. ISO Central Secretaria. 2009. Available online: https://www.iso.org/standard/36406.html (accessed on 28 April 2021).
28. ISO-10993-12. *Biological Evaluation of Medical Devices, Part 12: Sample Preparation and Reference Materials*. International Organization for Standardization, ISO Central Secretaria. 2012. Available online: https://www.iso.org/standard/53468.html (accessed on 28 April 2021).

29. Levy, G.K.; Ventura, Y.; Goldman, J.; Vago, R.; Aghion, E. Cytotoxic characteristics of biodegradable EW10X04 Mg alloy after Nd coating and subsequent heat treatment. *Mater. Sci. Eng. C* **2016**, *62*, 752–761. [CrossRef]
30. Liva and Dead Assay Manufacturer's Protocol. Abcam. 2019. Available online: https://www.abcam.com/ps/products/115/ab115347/documents/ab115347%20Live%20and%20Dead%20Cell%20Assay_30%20Jun%2015b%20(website).pdf (accessed on 28 April 2021).
31. Khamaj, J.A. Cyclic polarization analysis of corrosion behavior of ceramic coating on 6061 Al/SiC p composite for marine applications. *Prot. Met. Phys. Chem. Surf.* **2016**, *52*, 886–893. [CrossRef]
32. Arnon, A.; Aghion, E. Stress Corrosion Cracking of Nano/Sub-micron E906 Magnesium Alloy. *Adv. Eng. Mater.* **2008**, *10*, 742–745. [CrossRef]
33. Shearier, E.R.; Bowen, P.K.; He, W.; Drelich, A.; Drelich, J.; Goldman, J.; Zhao, F. In vitro cytotoxicity, adhesion, and proliferation of human vascular cells exposed to zinc. *ACS Biomater. Sci. Eng.* **2016**, *2*, 634–642. [CrossRef]
34. Li, Q.; Wei, M.; Yang, J.; Zhao, Z.; Ma, J.; Liu, D.; Lan, Y. Effect of Ca addition on the microstructure, mechanical properties and corrosion rate of degradable Zn-1Mg alloys. *J. Alloy. Compd.* **2021**, *887*, 161255. [CrossRef]
35. Chen, L.; Sheng, Y.; Wang, X.; Zhao, X.; Liu, H.; Li, W. Effect of Microstructure and Distribution of the Second Phase on the Stress Corrosion Cracking of Biodegradable Mg-Zn-Zr-xSr Alloys. *Materials* **2018**, *11*, 551. [CrossRef]
36. Merson, D.; Vasilev, E.; Markushev, M.; Vinogradov, A. On the corrosion of ZK60 magnesium alloy after severe plastic deformation. *Lett. Mater.* **2017**, *7*, 421–427. [CrossRef]
37. Aghion, E.; Levy, G.; Ovadia, S. In-vivo behavior of biodegradable Mg-Nd-Y-Zr-Ca alloy. *J. Mater. Sci. Mater. Med.* **2012**, *23*, 805–812. [CrossRef] [PubMed]
38. Thian, E.S.; Konishi, T.; Kawanobe, Y.; Lim, P.N.; Choong, C.; Ho, B.; Aizawa, M. Zinc-substituted hydroxyapatite: A biomaterial with enhanced bioactivity and antibacterial properties. *J. Mater. Sci. Mater. Med.* **2013**, *24*, 437–445. [CrossRef] [PubMed]
39. Wei, Z.; Burwinkel, M.; Palissa, C.; Ephraim, E.; Schmidt, M.F. Antiviral activity of zinc salts against transmissible gastroenteritis virus in vitro. *Vet. Microbiol.* **2012**, *160*, 468–472. [CrossRef]
40. Li, H.; Pang, S.; Liu, Y.; Sun, L.; Liaw, P.K.; Zhang, T. Biodegradable Mg–Zn–Ca–Sr bulk metallic glasses with enhanced corrosion performance for biomedical applications. *Mater. Des.* **2015**, *67*, 9–19. [CrossRef]